Materials Research Proceedings 41 (2024) 2144-2153 https://doi.org/10.21741/9781644903131-236

A new view on the solution of rate-independent crystal plasticity finite element models

NIJHUIS Björn[1,a*], PERDAHCIOĞLU Semih[1,b] and VAN DEN BOOGAARD Ton[1,c]

[1]Chair of Nonlinear Solid Mechanics, University of Twente, Enschede, The Netherlands

[a]b.nijhuis@utwente.nl, [b]e.s.perdahcioglu@utwente.nl, [c]a.h.vandenboogaard@utwente.nl

Keywords: Crystal Plasticity, Stress Update Algorithm, Active Set, Fixed-Point Iterations

Abstract. The crystal plasticity finite element method (CP-FEM) readily enables microstructure-based material modelling by relating macroscopic plastic deformation to dislocation slip on crystal slip systems. Rate-independent CP models provide physically accurate solutions by allowing slip only if the resolved shear stress on a slip system equals the critical resolved shear stress. However, computing the amount of slip for such models remains challenging. This work proposes a novel stable and efficient stress-update algorithm based on fixed-point iterations. These iterations trace the hypersurfaces that describe the slip state for which individual slip system's yield functions are zero, until all slip system hypersurfaces intersect. This simultaneously provides the set of active slip systems and the slip on these systems, avoiding the need for an iterative active set search algorithm without inducing spurious slip on systems on which the shear stress is below the critical resolved shear stress.

Introduction

The crystal plasticity finite element method (CP-FEM) is a powerful tool for incorporating microstructural effects into predictions of macroscopic mechanical behaviour of polycrystalline materials. CP-FEM models plastic deformation as the result of the combined slip activity on the material's crystallographic slip systems, requiring the amount of slip to be computed given the applied loading.

For deformations at low temperature, rate-independent CP models provide physically accurate solutions by allowing slip only if the resolved shear stress (RSS) on a slip system equals the critical resolved shear stress (CRSS) [1]. Active and inactive slip systems must then be distinguished, but the selection of the active set is nontrivial as it is not uniquely defined at start of an increment [2]. Therefore, stress update algorithms for rate-independent CP-FEM may start with a guess for the active set and compute the slip on the systems in that set, after which the active set is updated and slip computations are restarted if the resulting stress state requires slip systems to be (de)activated [3]. Such iterative search procedures clearly limit the computational efficiency of rate-independent CP models. As such, various authors introduced more sophisticated algorithms to initialize the active set [4-6].

The complexity of determining an active set led to the development of multiple CP formulations that do not require an active set at all. One approach is to relate the resolved and critical resolved shear stresses of all systems in a single yield function that defines a yield surface with rounded corners [7]. It is, however, difficult to incorporate effects of slip system interactions, e.g. latent hardening, in such a model [8].

A popular method that also does not require an active set, but does easily allow to include slip system interactions, is to employ viscoplastic regularisation and relate the slip activity of a slip system to the ratio between its RSS and CRSS [9]. This, however, renders the model rate-dependent and results in small amounts of slip on systems on which the RSS does not exceed the CRSS. An increase in plastic deformation may then cause extra hardening. Choosing model

parameters that result in a lower strain-rate sensitivity reduces the spurious slips, but also results in an ill-conditioned system of equations [10].

Recently proposed stress update algorithms based on the interior point method also avoid the active set search by rendering all slip systems active [11, 12]. These algorithms result in a truly rate-independent response, but alike viscoplastic models, induce slip even if the RSS on a system is below its CRSS.

This work aims at developing a novel stress-update algorithm for rate-independent CP models that does not require an active set search procedure and does not induce spurious slip on systems on which the RSS is lower than the CRSS. We first formulate the rate-independent crystal plasticity model, after which we propose a stress-update algorithm based on fixed-point iterations. Then, we demonstrate the feasibility of this algorithm and compare its stability with that of a conventional Newton-Raphson based stress update algorithm for rate-independent CP.

Formulation of the crystal plasticity model

We take as the starting point for the formulation of the CP model the multiplicative decomposition of the deformation gradient tensor $\mathbf{F}$ into an elastic ($\mathbf{F}_\mathrm{e}$) and a plastic part $\left(\mathbf{F}_\mathrm{p}\right)$ as

$$\mathbf{F} = \mathbf{F_e} \cdot \mathbf{F}_\mathrm{p} \,. \tag{1}$$

Here, $\mathbf{F}_\mathrm{p}$ defines an intermediate configuration that results from plastic slip caused by dislocation motion and in which the crystal lattice is undistorted. $\mathbf{F}_\mathrm{e}$ accounts for the rotation and elastic stretch of the lattice and relates this intermediate configuration to the current configuration. In the following, an overset hat ($\hat{}$) is used to denote symbols that are mapped from the intermediate to the current configuration. The total velocity gradient $\mathbf{L} = \dot{\mathbf{F}} \cdot \mathbf{F}^{-1}$ can now be additively decomposed into its elastic ($\hat{\mathbf{L}}_\mathrm{e}$) and plastic $\left(\hat{\mathbf{L}}_\mathrm{p}\right)$ components as

$$\mathbf{L} = \hat{\mathbf{L}}_\mathbf{e} + \hat{\mathbf{L}}_\mathrm{p}, \tag{2}$$

while the plastic deformation gradient is given by a summation of the plastic slip rates on the crystal's n_s slip systems as

$$\hat{\mathbf{L}}_\mathrm{p} = \sum_{\alpha=1}^{n_\mathrm{s}} \dot{\boldsymbol{\gamma}}^{(\alpha)}\, \hat{\mathbf{s}}^{(\alpha)} \otimes \hat{\mathbf{m}}^{(\alpha)}. \tag{3}$$

Here, $\dot{\boldsymbol{\gamma}}^{(\alpha)}$ is the plastic slip rate on a slip system α that is defined by the unit slip direction vector $\hat{\mathbf{s}}^{(\alpha)}$ and unit slip plane normal vector $\hat{\mathbf{m}}^{(\alpha)}$. In this work, we consider a face centred cubic (FCC) lattice.

In a rate-independent CP model, slip on a system α is allowed only if the resolved shear stress $\tau_\mathrm{r}^{(\alpha)}$ on that system equals the critical resolved shear stress $\tau_\mathrm{f}^{(\alpha)}$. The resolved shear stress $\tau_\mathrm{r}^{(\alpha)}$ is calculated by projecting the stress $\boldsymbol{\sigma}$ as

$$\tau_\mathrm{r}^{(\alpha)} = \boldsymbol{\sigma} : \hat{\mathbf{P}}^{(\alpha)} = \boldsymbol{\sigma} : \frac{1}{2}\left(\hat{\mathbf{s}}^{(\alpha)} \otimes \hat{\mathbf{m}}^{(\alpha)} + \hat{\mathbf{m}}^{(\alpha)} \otimes \hat{\mathbf{s}}^{(\alpha)}\right), \tag{4}$$

where $\hat{\mathbf{P}}^{(\alpha)}$ denotes the symmetric Schmid tensor. We compute the critical resolved shear stress $\tau_\mathrm{f}^{(\alpha)}$ using a Taylor type hardening law as

$$\tau_\mathrm{f}^{(\alpha)} = \tau_0 + Gb\sqrt{\sum_{\beta=1}^{n_\mathrm{s}} Q^{(\alpha\beta)} \rho^{(\beta)}}. \tag{5}$$

Here, τ_0 represents a constant lattice friction, G is the shear modulus and b is the length of the Burgers vector. The component $Q^{(\alpha\beta)}$ of the interaction matrix $\mathbf{Q}$ determines the hardening of slip system α as a result of an increase in dislocation density $\rho^{(\beta)}$ on slip system β. The components of $\mathbf{Q}$ are governed by six independent types of slip system interactions [13], as listed in Table 1, for which the coefficients are taken from results of dislocation dynamics analysis conducted by Kubin et al. [13]. The relation between the dislocation density and the accumulated plastic slip $\gamma^{(\alpha)} = \int_{t_0}^{t_{\mathrm{end}}} \left|\dot{\gamma}^{(\alpha)}\right| dt$ on a slip system α is modelled with the phenomenological constitutive model given by Becker [14]:

$$\rho^{(\alpha)} = \rho_\infty \left[1 - \left(1 - \frac{\rho_0}{\rho_\infty}\right) \exp(-\frac{\gamma^\alpha}{\gamma_\infty})\right]. \tag{6}$$

Here, ρ_0, ρ_∞ and γ_∞ are the initial dislocation density, saturation dislocation density and saturation slip, respectively. The values for the constants in Eqs. 5 and 6 are provided in Table 2.

Table 1: Coefficients for slip system interactions in an FCC lattice [13]

Self	*Coplanar*	*Collinear*	*Orthogonal*	*Glissile*	*Sessile*
0.122	*0.122*	*0.625*	*0.070*	*0.137*	*0.122*

Table 2: Model parameters used in Eqs. 5 and 6 [12]

E [GPa]	*ν [-]*	*τ_0 [MPa]*	*b [mm]*	*ρ_0 [mm-2]*	*ρ_∞ [mm-2]*	*γ_∞ [-]*
72.0	*0.3*	*18.0*	*2.86×10-7*	*107*	*109*	*0.4*

Fixed-point iteration scheme for slip computations

Now, we will formulate a stress update algorithm that provides the increments of stress and plastic slip on the crystal's slip systems during a time increment from t_n to $t_{n+1} = t_n + \Delta t$ as function of the total rate of deformation tensor $\mathbf{D}$ (the symmetric part of $\mathbf{L}$, Eq. 2). A trial stress state is given as

$$\boldsymbol{\sigma}^*_{n+1} = \boldsymbol{\sigma}_n + \hat{\mathbb{C}}_\mathrm{e} : \Delta\mathbf{D}. \tag{7}$$

Here, $\hat{\mathbb{C}}_\mathrm{e}$ denotes the elasticity tensor of the lattice in the current configuration. If for at least one slip system the RSS resulting from the trial stress state exceeds the CRSS, the closest point projection (CPP) from the trial state onto the yield surface is computed. The nonlinear systems of equations that defines this projection can be derived using the principle of maximum dissipation. For a detailed treatment of this derivation, the reader is referred to [12]. It follows that for all active slip systems, which define the active set A, it has to hold that

$$\mathbf{R}_\sigma = \hat{\mathbb{C}}_\mathrm{e} : \Delta\mathbf{D} - \Delta\boldsymbol{\sigma} - \hat{\mathbb{C}}_\mathrm{e} : \sum_{\alpha\in A} \widehat{\mathbf{P}}^{(\alpha)} \Delta\gamma^{(\alpha)} = \mathbf{0}, \tag{8}$$

$$\phi^{(\alpha)} = \tau_\mathrm{r}^{(\alpha)} - \tau_\mathrm{f}^{(\alpha)} = 0 \qquad \forall\alpha \in A, \tag{9}$$

while for all systems that are not in the active set it has to hold that

$$\phi^{(\alpha)} = \tau_\mathrm{r}^{(\alpha)} - \tau_\mathrm{f}^{(\alpha)} < 0 \qquad \forall\alpha \in N. \tag{10}$$

Here, $N = T \setminus A$ denotes the set of inactive systems, with T being the set of all n_s slip systems. In Eq. 8, it is used that $\Delta\gamma^{(\alpha)} = \dot{\gamma}^{(\alpha)}\Delta\mathrm{t}$ and $\Delta\mathbf{D} = \mathbf{D}\Delta\mathrm{t}$.

A common approach to solve the system given by Eqs. 8 and 9 is to linearise these equations and iteratively update the increments of plastic slip on the active systems and the stress using the Newton-Raphson (NR) algorithm [2, 3, 10]. This, clearly, requires the active set A to be established. If the conditions in Eqs. 9 and 10 cannot be satisfied for a given active set, it has to be updated and the NR iterations have to be restarted.

To avoid having to explicitly initialise and update the active set during a time increment, we propose to combine Eqs. 9 and 10 into a single condition that has to hold for each slip system:

$$\tilde{\phi}^{(\alpha)} = \tau_{\mathrm{r}}^{(\alpha)} - \tilde{\tau}_{\mathrm{f}}^{(\alpha)} = 0 \qquad \forall \alpha \in T, \tag{11}$$

for which a modified flow stress is defined as

$$\tilde{\tau}_{\mathrm{f}}^{(\alpha)} = \begin{cases} \tau_{\mathrm{r}}^{(\alpha)} & \text{if } \gamma^{(\alpha)} = 0 \wedge \left|\tau_{\mathrm{R}}^{(\alpha)}(\Delta\mathbf{D}, \Delta\boldsymbol{\gamma})\right| < \tau_{\mathrm{f}}^{(\alpha)}(\boldsymbol{\gamma}_n, \Delta\boldsymbol{\gamma}) \\ \mathrm{sign}\left(\gamma^{(\alpha)}\right) \tau_{\mathrm{f}}^{(\alpha)}(\boldsymbol{\gamma}_n, \Delta\boldsymbol{\gamma}) & \text{otherwise} \end{cases}. \tag{12}$$

The condition in Eq. 11 can be rewritten in Mandel notation [15] as

$$\tilde{\phi}^{(\alpha)}(\Delta\mathbf{D}, \boldsymbol{\gamma}_n, \Delta\boldsymbol{\gamma}) = \underline{\widehat{\mathbf{P}}}^{(\alpha)\mathrm{T}} \underline{\boldsymbol{\sigma}}^*_{n+1}(\Delta\mathbf{D}) - \underline{\widehat{\mathbf{P}}}^{(\alpha)\mathrm{T}} \underline{\hat{\mathbb{C}}}_{\mathrm{e}} \underline{\widehat{\mathbf{P}}} \Delta\boldsymbol{\gamma} - \tilde{\tau}_{\mathrm{f}}^{(\alpha)}(\boldsymbol{\gamma}_n, \Delta\boldsymbol{\gamma}) = 0 \qquad \forall \alpha \in T, \tag{13}$$

using Eqs. 4 and 8 and noting that $\boldsymbol{\sigma}_{n+1} = \boldsymbol{\sigma}_n + \Delta\boldsymbol{\sigma}$. In Eq. 13 and the remainder of the text, all underlined symbols denote matrix and vector representations of tensors in Mandel notation. Column α of the matrix $\underline{\widehat{\mathbf{P}}}$ corresponds to the Mandel vector $\underline{\widehat{\mathbf{P}}}^{(\alpha)}$ of the symmetric Schmid tensor $\widehat{\mathbf{P}}^{(\alpha)}$ [12]. The vector $\boldsymbol{\gamma}_n$ contains the accumulated slips of all slip systems.

The solution $\Delta\bar{\boldsymbol{\gamma}}$ to Eq. 13 is located at an intersection of the n_{s} hypersurfaces $\tilde{\phi}^{(\alpha)}(\Delta\boldsymbol{\gamma}) = 0$. Each of these hypersurfaces defines where $\Delta\boldsymbol{\gamma}$ is such that the linear function

$$r^{(\alpha)}(\Delta\boldsymbol{\gamma}) = \underline{\widehat{\mathbf{P}}}^{(\alpha)\mathrm{T}} \underline{\hat{\mathbb{C}}}_{\mathrm{e}} \underline{\widehat{\mathbf{P}}} \Delta\boldsymbol{\gamma} \tag{14}$$

crosses the nonlinear function

$$g^{(\alpha)}(\Delta\mathbf{D}, \boldsymbol{\gamma}_n, \Delta\boldsymbol{\gamma}) = \underline{\widehat{\mathbf{P}}}^{(\alpha)\mathrm{T}} \underline{\boldsymbol{\sigma}}^*_{n+1}(\Delta\mathbf{D}) - \tilde{\tau}_{\mathrm{f}}^{(\alpha)}(\boldsymbol{\gamma}_n, \Delta\boldsymbol{\gamma}). \tag{15}$$

Due to the nature of the functions in Eqs. 14 and 15 and the definition of $\tilde{\tau}_{\mathrm{f}}^{(\alpha)}$ in Eq. 12, this crossing always occurs at $\left|\Delta\gamma^{(\alpha)}\right| > 0$ if $\left|\tau_{\mathrm{r}}^{(\alpha)}\right| = \tilde{\tau}_{\mathrm{f}}^{(\alpha)}$, and at $\gamma^{(\alpha)} = 0$ if $\left|\tau_{\mathrm{r}}^{(\alpha)}\right| < \tilde{\tau}_{\mathrm{f}}^{(\alpha)}$. Figures 1a and 1b show this schematically for an exemplary single crystal with two slip systems that is subjected to a tensile stress of 300 MPa. The two slip systems are oriented at an angle of -15° and 60° with respect to the tensile axis, respectively. The CRSS on both systems evolves as given by Eqs. 5 and 6. For this example only, $Q^{(\alpha\beta)} = 1.4 - 0.4\delta_{\alpha\beta}$, where $\delta_{\alpha\beta}$ is the Kronecker delta function. As seen in Figure 1c, an intersection of the hypersurfaces $\tilde{\phi}^{(\alpha)} = 0$ defines both the active set and the slip activity on the (active) slip systems.

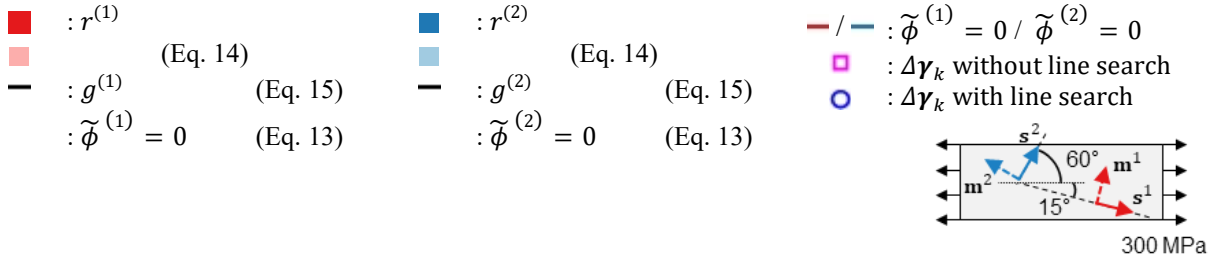

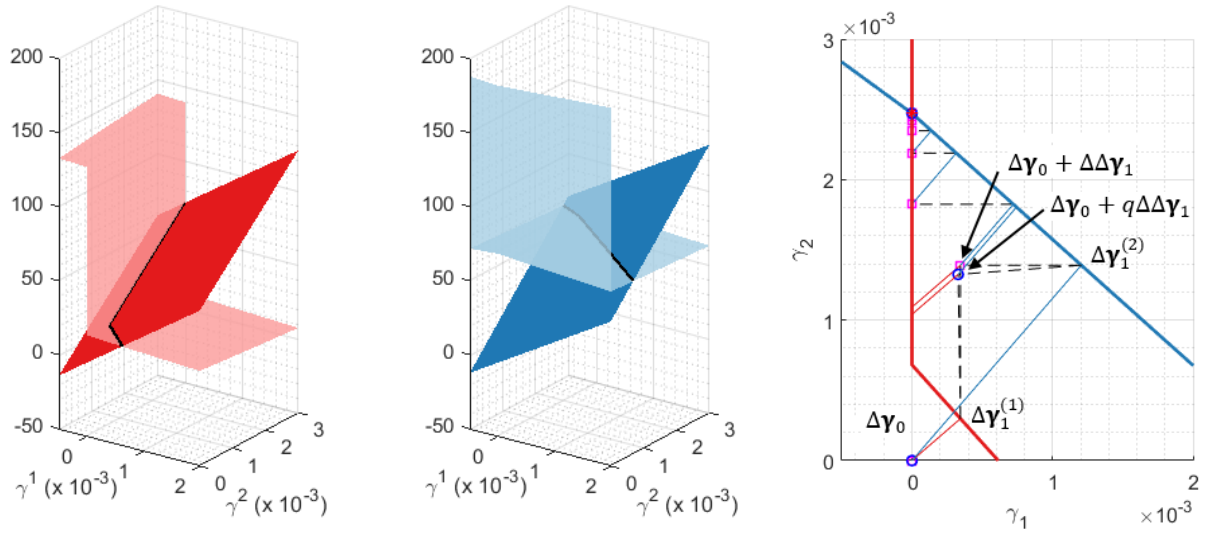

(a) System 1 *(b) System 2* *(c) Convergence of the FPI scheme towards* $\tilde{\phi}^{(1)} = \tilde{\phi}^{(2)} = 0$.

Figure 1: Visualisation of (a)-(b) the hypersurfaces $\tilde{\phi}^{(\alpha)} = 0$ *for the model shown top right and (c) the use of these hypersurfaces to determine the active set and slip activity.*

Based on this observation, we developed a novel fixed-point iteration (FPI) scheme that traces the hypersurfaces of the individual systems until it finds the fixed-point at which all n_s hypersurfaces intersect. Table 3 shows the pseudocode for the proposed FPI scheme. Figure 1c shows the progress of the fixed-point iterations to compute the slip on the two slip systems for the exemplary single crystal introduced above.

Given an estimate $\Delta\boldsymbol{\gamma}_k$ for $\Delta\bar{\boldsymbol{\gamma}}$, the FPI scheme performs two main steps. In the first step, n_s one-dimensional root-finding problems are solved. Each solution provides the step length $t^{(\alpha)}$ for which the point $\Delta\boldsymbol{\gamma}_{k+1}^{(\alpha)} = \Delta\boldsymbol{\gamma}_k + \mathrm{t}^{(\alpha)}\mathbf{d}^{(\alpha)}$ is located on the hypersurface $\tilde{\phi}^{(\alpha)} = 0$. The search direction vector $\mathbf{d}^{(\alpha)}$ is chosen as the normalised α-th column of the symmetric matrix $\underline{\widehat{\mathbf{P}}}^{\mathrm{T}}\underline{\widehat{\mathbb{C}}}_{\mathrm{e}}\underline{\widehat{\mathbf{P}}}$. The results $\Delta\boldsymbol{\gamma}_{k+1}^{(\alpha)}$ are combined to compute the direction $\Delta\Delta\boldsymbol{\gamma}_{k+1}$ along which the slip increment will be updated by setting $\Delta\Delta\gamma_{k+1}^{(\alpha)} = \mathrm{t}^{(\alpha)}\mathrm{d}^{(\alpha\alpha)}$. Here, $\mathrm{d}^{(\alpha\alpha)}$ is the α-th component of the search direction vector $\mathbf{d}^{(\alpha)}$.

In the second step, a line search along $\Delta\Delta\boldsymbol{\gamma}_{k+1}$ is performed and $\Delta\boldsymbol{\gamma}_k$ is updated as $\Delta\boldsymbol{\gamma}_{k+1} = \Delta\boldsymbol{\gamma}_k + q\Delta\Delta\boldsymbol{\gamma}_{k+1}$. The step length $q > 0$ is chosen such as to minimise the L2-norm of the residual functions $\tilde{\phi}^{(\alpha)}(\Delta\boldsymbol{\gamma}_k + q\Delta\Delta\boldsymbol{\gamma}_{k+1})$ of all currently active slip systems. The positive influence of this line search step on the convergence behaviour of the FPI scheme can be clearly observed in Figure 1c. When the line search step is enabled, the number of iterations to compute the slip activity of the exemplary single crystal reduces from 17 to only 2.

The one-dimensional root-finding and the scalar minimisation problem are solved by the general and standard algorithms given by Brent [16]. These algorithms require only function evaluations and simple bracketing operations and are therefore easily implemented and numerically cheap to evaluate.

The crystal lattice rotates during deformation. This requires to update $\underline{\widehat{\mathbf{P}}}^{(\alpha)}$ and $\underline{\widehat{\mathbb{C}}}_{\mathrm{e}}$ during iterations. These updates are implemented as described in [12]. Allowing the lattice to rotate during iterations causes the fixed-point to move during the iterations. The influence thereof on the convergence of the FPI scheme will be analysed in the result section below.

After convergence of the FPI scheme, Eqs. 8 and 9 hold for all active slip systems. As such, the stress increment can be computed using Eq. 8 as

$$\Delta\underline{\boldsymbol{\sigma}} = \underline{\hat{\mathbb{C}}}_{\mathrm{e}}\Delta\underline{\mathbf{D}} - \hat{\mathbb{C}}_{\mathrm{e}}\underline{\hat{\mathbf{P}}}\Delta\boldsymbol{\gamma}, \tag{16}$$

and the consistent algorithmic tangent $\underline{\mathbb{C}}_{\mathrm{ep}}$ can be derived as [12]

$$\underline{\mathbb{C}}_{\mathrm{ep}} = \left(\underline{\hat{\mathbb{C}}}_{\mathrm{e}}^{-1} + \underline{\hat{\mathbf{P}}}\mathbf{G}^{-1}\underline{\hat{\mathbf{P}}}^{\mathrm{T}}\right)^{-1}. \tag{17}$$

Here, $G^{(\alpha\beta)} = \partial\phi^{(\alpha)}/\partial\gamma^{(\beta)}$.

Table 3: Fixed-point iteration based stress update algorithm for rate-independent CP

1. Initialisation:

$k \leftarrow 0$

$\Delta\boldsymbol{\gamma}_k \leftarrow \mathbf{0}$

Compute lattice rotation, update $\underline{\hat{\mathbb{C}}}_{\mathrm{e}}$ and Schmid tensors $\underline{\hat{\mathbf{P}}}^{(\alpha)}$

Set search directions: $\mathbf{d}^{(\alpha)} \leftarrow$ normalised α-th column of $\underline{\hat{\mathbf{P}}}^{\mathrm{T}}\underline{\hat{\mathbb{C}}}_{\mathrm{e}}\underline{\hat{\mathbf{P}}}$

$\underline{\boldsymbol{\sigma}}_{n+1}^{*} \leftarrow \underline{\boldsymbol{\sigma}}_n + \underline{\hat{\mathbb{C}}}_{\mathrm{e}}\Delta\underline{\mathbf{D}}$

$r_0 = \min\left(1.0\,, \sqrt{\sum_{\alpha\in A_k}\left(\left|\underline{\hat{\mathbf{P}}}^{(\alpha)^{\mathrm{T}}}\underline{\boldsymbol{\sigma}}_{n+1}^{*}\right| - \tau_{\mathrm{f}}^{(\alpha)}\right)^2}\right)$, $A_k = \left\{\alpha \in T : \left|\tau_{\mathrm{r}}^{(\alpha)}\right| > \tau_{\mathrm{f}}^{(\alpha)}\right\}$

$r \leftarrow r_0$

2. FPI-iterations:

do while $r > 10^{-4}$

$k \leftarrow \mathrm{k} + 1$

for $\alpha = 1, 2, \ldots, n_{\mathrm{s}}$ do

find $t^{(\alpha)}$: solve $\widetilde{\phi}^{(\alpha)}\left(\boldsymbol{\gamma}_n, \Delta\boldsymbol{\gamma}_{k-1} + \mathrm{t}^{(\alpha)}\mathbf{d}^{(\alpha)}\right) = 0$

$\Delta\Delta\gamma_k^{(\alpha)} \leftarrow \mathrm{t}^{(\alpha)}\mathrm{d}^{(\alpha\alpha)}$

for $\alpha = 1, 2, \ldots, n_{\mathrm{s}}$ do

if $\Delta\gamma_{k-1}^{(\alpha)} + \Delta\Delta\gamma_k^{(\alpha)} = 0$:

$\Delta\gamma_{k-1}^{\alpha} \leftarrow 0$

$\Delta\Delta\gamma_k^{(\alpha)} \leftarrow 0$

find q: minimize $\sqrt{\sum_{\alpha\in A_k}\widetilde{\phi}^{(\alpha)}\left(\boldsymbol{\gamma}_n, \Delta\boldsymbol{\gamma}_{k-1} + q\Delta\Delta\boldsymbol{\gamma}_k\right)^2}$, $A_k = \left\{\alpha \in T: \left|\tau_{\mathrm{r}}^{(\alpha)}\right| > \tau_{\mathrm{f}}^{(\alpha)} \vee \left|\Delta\boldsymbol{\gamma}_{k-1} + q\Delta\Delta\boldsymbol{\gamma}_k\right| > 0\right\}$

if $q > 0$:

$\Delta\Delta\gamma_k^{(\alpha)} \leftarrow q\Delta\Delta\boldsymbol{\gamma}_k$

$\Delta\boldsymbol{\gamma}_k \leftarrow \Delta\boldsymbol{\gamma}_{k-1} + \Delta\Delta\boldsymbol{\gamma}_k$

Compute lattice rotation, update $\underline{\hat{\mathbb{C}}}_{\mathrm{e}}$ and Schmid tensors $\underline{\hat{\mathbf{P}}}^{(\alpha)}$

Set search directions: $\mathbf{d}^{(\alpha)} \leftarrow$ normalised α-th column of $\underline{\hat{\mathbf{P}}}^{\mathrm{T}}\underline{\hat{\mathbb{C}}}_{\mathrm{e}}\underline{\hat{\mathbf{P}}}$

$\underline{\boldsymbol{\sigma}}_{n+1}^{*} \leftarrow \underline{\boldsymbol{\sigma}}_n + \underline{\hat{\mathbb{C}}}_{\mathrm{e}}\Delta\underline{\mathbf{D}}$

$r \leftarrow \sqrt{\sum_{\alpha\in A_k}\left(\left|\underline{\hat{\mathbf{P}}}^{(\alpha)^{\mathrm{T}}}\underline{\boldsymbol{\sigma}}_{n+1}^{*} - \underline{\hat{\mathbf{P}}}^{(\alpha)^{\mathrm{T}}}\underline{\hat{\mathbb{C}}}_{\mathrm{e}}\underline{\hat{\mathbf{P}}}\Delta\boldsymbol{\gamma}\right| - \tau_{\mathrm{f}}^{(\alpha)}\right)^2}$, $A_k = \left\{\alpha \in T: \left|\tau_{\mathrm{r}}^{(\alpha)}\right| > \tau_{\mathrm{f}}^{(\alpha)} \vee \left|\Delta\boldsymbol{\gamma}_k\right| > 0\right\}$

3. Stress update and algorithmic tangent computation:

$\underline{\boldsymbol{\sigma}}_{n+1} = \underline{\boldsymbol{\sigma}}_n + \underline{\hat{\mathbb{C}}}_{\mathrm{e}}\Delta\underline{\mathbf{D}} - \hat{\mathbb{C}}_{\mathrm{e}}\underline{\hat{\mathbf{P}}}\Delta\boldsymbol{\gamma}$

$\underline{\hat{\mathbb{C}}}_{\mathrm{ep}} = \left(\underline{\hat{\mathbb{C}}}_{\mathrm{e}}^{-1} + \underline{\hat{\mathbf{P}}}\mathbf{G}^{-1}\underline{\hat{\mathbf{P}}}^{\mathrm{T}}\right)^{-1}$

Materials Research Proceedings 41 (2024) 2144-2153 https://doi.org/10.21741/9781644903131-236

Results and discussion

In this section, the stability of the novel FPI-based stress update algorithm will be assessed. Its behaviour is compared against that of a conventional Newton Raphson (NR)-based CPP algorithm with an iterative active set update procedure. The NR-based algorithm, implemented as described in [12], has two options to initialise the active set at the start of the increment. It could (i) be initialised as the active set of the previous increment or (ii) include all systems for which the trial stress renders $\tau_{\mathrm{r}}^{(\alpha)} > \tau_{\mathrm{f}}^{(\alpha)}$. Analyses with the NR-based algorithm are aborted if an update to the active set results in a set that has already been tried (and failed) during an increment. Both algorithms are implemented in a FORTRAN module that returns the increments of stress and plastic slip of a material point for a given deformation increment. All analyses below are conducted for an initially stress-free FCC single crystal of which the lattice coordinate system is aligned with the global coordinate system at the start of the analysis.

Stability of the solution scheme for a deformation-driven problem. We first consider a simple shear test in which a material point is deformed by prescribing a total deformation gradient tensor with $F_{12} = 4.0$ in 10, 100 and 1000 increments. Solutions are attempted with both the FPI-based and the NR-based algorithm. For the latter, a converged solution was only reached for the test with 1000 increments using option (ii) to initialise the active set. The FPI-based algorithm, on the other hand, converged for all increment counts considered.

Figure 2 shows the resulting stress-strain curves. The solutions obtained with the FPI scheme stably converge with an increasing number of increments. For the simulation with 1000 increments, the FPI-based algorithm yields the same result as the NR-based algorithm. The fact that the FPI-based algorithm correctly predicted the material response in as little as 10 increments shows that it converges to a solution even in the presence of large rotations. The FPI scheme thus allows for a large increment size.

Figure 2 furthermore shows that only very few fixed-point iterations per increment are required during the simulations with 100 and 1000 increments. At 1000 increments, the average number of fixed-point iterations is comparable to the average number of NR-iterations. Recall that each fixed-point iteration requires only function evaluations and simple bracketing operations to compute the solution to the 12 (for FCC) one-dimensional root-finding problems (line 11 of Table 3) and the scalar optimisation problem (line 17 of Table 3), whereas an iteration with the NR-based algorithm requires to solve a system of equations of which the size equals the number of active slip systems. For the simple shear problem solved in 1000 increments, the average number of iterations in solving each root-finding problem is only 11, that to solve the scalar optimisation problem is 23, while the number of active system in the majority of the increments equals 8. These numbers and the iteration counts in Figure 2 indicate that the novel FPI scheme can be competitive with a conventional NR-based stress update scheme, especially when the latter requires multiple restarts due to the iterative active set search. A more detailed analysis of the computational time is, however, required to further asses the performance of the FPI scheme.

Influence of lattice rotations. To investigate the effect of lattice rotations on the convergence behaviour of the FPI scheme, we reran the simple shear test with 10 and 100 increments while turning off the lattice rotations during the fixed-point iterations (Lines 21 – 23 in Table 3). Rotations are now updated in a staggered manner only after convergence of the FPI scheme.

For the simulation with 100 increments, the resulting stress-strain curve in Figure 3 lags only slightly behind that of the corresponding analysis in which lattice rotations during the fixed-point iterations were enabled. For the simulation with 100 increments, lattice rotations during each increment are thus small. Figure 3 shows that in such a case, enabling lattice rotations during the fixed-point iterations does not significantly affect the number of fixed-point iterations.

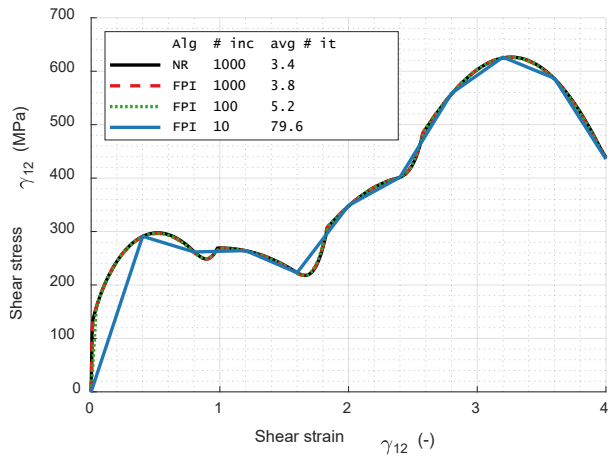

Figure 2: Stress – strain curves for a single crystal under simple shear deformation, prescribed in 10, 100 and 1000 increments, as predicted by a conventional NR-based [12] and the proposed FPI-based stress update algorithm, along with the average number of NR or FPI iterations per increment.

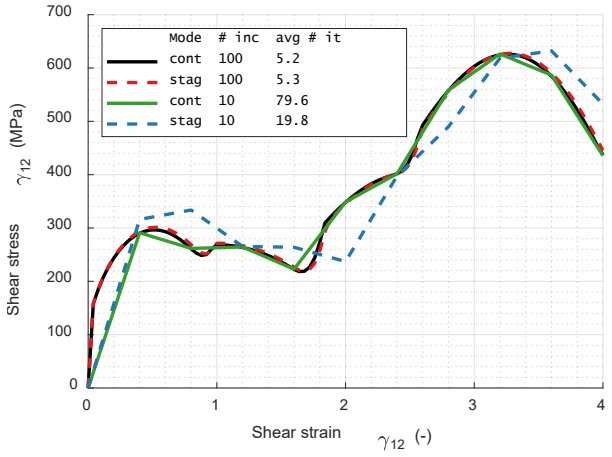

Figure 3: Stress – strain curves for a single crystal under simple shear deformation, prescribed in 10 and 100 increments, as predicted by the proposed FPI-based stress update algorithm with (Mode = cont) and without (Mode = stag) rotation updates during the FPI-iterations, along with the average number of FPI iterations per increment.

This is different for the simulation with 10 increments. The resulting stress-strain curve in Figure 3 differs significantly from that of the corresponding analysis with lattice rotations during the fixed-point iterations enabled. This indicates that the fixed-point now moves considerably during the iterations. Clearly, staggered rotation updates do not yield accurate results for such a limited number of increments. Nonetheless, for this test, enabling rotation updates during fixed-point iterations increases the average number of fixed-point iterations by a factor four. Severe lattice rotations within an increment could thus slow down the convergence of the FPI scheme.

Stability of the solution scheme for a stress-driven problem. The tests considered so far were deformation-driven. As such, no global equilibrium iterations were needed to obtain a converged solution. To assess the stability of the proposed FPI-based stress update algorithm within such equilibrium iterations, we now consider a stress-driven problem.

For this problem, the incremental deformation rate $\Delta\underline{\mathbf{D}}_n$ that produces the prescribed stress $\underline{\mathbf{s}}_{n+1}$ at the end of an increment n has to be iteratively computed. At the end of the k^{th} equilibrium iteration, $\Delta\underline{\mathbf{D}}_n$ is updated as $\Delta\underline{\mathbf{D}}_n^{k+1} = \Delta\underline{\mathbf{D}}_n^k + \Delta\Delta\underline{\mathbf{D}}_n^k$, with $\Delta\Delta\underline{\mathbf{D}}_n^k = \underline{\mathbb{C}}_{\text{ep}}^{-1}\left(\underline{\mathbf{s}}_{n+1} - \underline{\mathbf{s}}^k\right)$. The bracketed term in the last expression is the difference between the prescribed stress state and the stress as currently predicted by the stress update algorithm. Equilibrium iterations continue while the magnitude of the largest element in $\left(\underline{\mathbf{s}}_{n+1} - \underline{\mathbf{s}}^k\right)$ is larger than 10^{-3} times the magnitude of the largest element in the initial difference vector $\left(\underline{\mathbf{s}}_{n+1} - \underline{\mathbf{s}}^1\right)$.

We considered a total of 968 different load cases in which the normal components of the stress tensor are prescribed. These components are given by 968 points that are evenly distributed on a sphere with a radius of 400 MPa to cover a large space of possible load directions. The Fibonacci lattice [17] is used to distribute the points. Each load case is applied in 10 increments and solved both with the FPI-based and the NR-based stress update algorithms. The FPI-based algorithm converged in 96.3% of the cases, whereas the NR-based algorithm converged in only 76.4% of the cases. For this stress-drive problem, the NR-based algorithm was found to converge best when using option (i) to initialise the active set.

The fact that not all load cases have converged is caused by a well-known property of rate-independent CPP algorithms. If the active set changes during equilibrium iterations, the resulting changes in the algorithmic tangent can lead to non-convergence of these iterations [18]. The FPI scheme still uses an active set and hence is not invulnerable to this behaviour. Nonetheless, it does not suffer from breakdowns of the iterative active set search procedure that cause the NR-based algorithm to abort prematurely, and therefore allows more of the load cases to converge. Given that the FPI scheme is able to resolve the vast majority of load cases, it seems a promising alternative to CPP algorithms with iterative active set search.

Conclusion

A novel stress update algorithm for rate-independent crystal plasticity was presented in this work. It was developed based on the observation that the set of active slip systems does not have to be explicitly initialised and updated if, for each of the crystal's n_s slip systems, a single condition is formulated that has to be zero both when the system is active as well as when it is inactive. The slip state for which each of these conditions is zero is defined by a hypersurface in n_s-dimensional space. We proposed a fixed-point iteration (FPI) scheme to trace these hypersurfaces until they all intersect. The resulting stress update algorithm simultaneously provides the set of active slip systems and their slip activity, without inducing spurious stresses on nonactive systems. It stably converges to a solution even when the crystal lattice rotates significantly during iterations, allowing for large increment sizes. The proposed stress update algorithm is furthermore shown to be efficient and significantly more stable than a conventional Newton-Raphson-based stress update scheme featuring an iterative active set search procedure.

References

[1] H. K. Akpama, M. B. Bettaieb, F. Abed-Meraim, Numerical integration of rate-independent BCC single crystal plasticity models: comparative study of two classes of numerical algorithms, Int J Numer Meth Eng, 108:5 (2016) 363-422. https://doi.org/10.1002/nme.5215

[2] C. Miehe, J. Schröder, A comparative study of stress update algorithms for rate-independent and rate-dependent crystal plasticity, Int J Numer Meth Eng, 50:2 (2001) 273-298. https://doi.org/10.1002/1097-0207(20010120)50:2<273::AID-NME17>3.3.CO;2-H

[3] C. Miehe, J. Schotte, Crystal Plasticity and Evolution of Polycrystalline Microstructure, in: E. Stein, R. De Borst, and T. J. R. Hughes (Eds.), Encyclopedia of Computational Mechanics Second Edition, John Wiley & Sons, Ltd. 2004, pp. 267-289.

[4] R. McGinty, D. McDowell, A semi-implicit integration scheme for rate independent finite crystal plasticity, Int J Plasticity, 22:6 (2006) 996-1025. https://doi.org/10.1016/j.ijplas.2005.06.002

[5] C. Miehe, D. Rosato, Fast texture updates in fcc polycrystal plasticity based on a linear active-set-estimate of the lattice spin, J Mech Phys Solids, 55:12 (2007) 2687-2716. https://doi.org/10.1016/j.jmps.2007.04.002

[6] M. Ben Bettaieb, O. Débordes, A. Dogui, L. Duchêne, C. Keller, On the numerical integration of rate independent single crystal behavior at large strain, Int J Plasticity, 32-33 (2012) 184-217. https://doi.org/10.1016/j.ijplas.2011.10.010

[7] T. Mánik, H. M. Asadkandi, B. Holmedal, A robust algorithm for rate-independent crystal plasticity, Comput Meth Appl Mech Eng, 393 (2022) 114831. https://doi.org/10.1016/j.cma.2022.114831

[8] S. Forest, M. B. Rubin, A rate-independent crystal plasticity model with a smooth elastic–plastic transition and no slip indeterminacy, Eur J Mech A-Solid, 55 (2016) 278-288. https://doi.org/10.1016/j.euromechsol.2015.08.012

[9] F. Roters, P. Eisenlohr, T. R. Bieler, D. Raabe, Crystal Plasticity Finite Element Methods in Materials Science and Engineering. Wiley-VCH Verlag GmbH & Co. KGaA, Weinheim, 2010. https://doi.org/10.1002/9783527631483

[10] M. Schmidt-Baldassari, Numerical concepts for rate-independent single crystal plasticity, Comput Meth Appl Mech Eng, 192:11-12 (2003) 1261-1280. https://doi.org/10.1016/S0045-7825(02)00563-7

[11] L. Scheunemann, P. S. B. Nigro, J. Schröder, P. M. Pimenta, A novel algorithm for rate independent small strain crystal plasticity based on the infeasible primal-dual interior point method, Int J Plasticity, 124 (2020) 1-19. https://doi.org/10.1016/j.ijplas.2019.07.020

[12] E. S. Perdahcıoğlu, A rate-independent crystal plasticity algorithm based on the interior point method, Comput Meth Appl Mech Eng, 418 (2024) 116533. https://doi.org/10.1016/j.cma.2023.116533

[13] L. P. Kubin, B. Devincre, M. Tang, Mesoscopic modelling and simulation of plasticity in fcc and bcc crystals: Dislocation intersections and mobility, J Comput-Aided Mater Des, 5:1 (1998) 31-54. https://doi.org/10.1023/A:1008648120261

[14] M. Becker, "Incompatibility and Instability Based Size Effects in Crystals and Composites at Finite Elastoplastic Strains," PhD-thesis, Universität Stuttgart, Stuttgart, 2006.

[15] J. Mandel, Generalisation de la theorie de plasticite de W. T. Koiter, Int J Solids Struct, 1:3 (1965) 273-295. https://doi.org/10.1016/0020-7683(65)90034-X

[16] R. P. Brent, Algorithms for Minimization without Derivatives. Prentice-Hall, New Jersey, 1973.

[17] Á. González, Measurement of Areas on a Sphere Using Fibonacci and Latitude–Longitude Lattices, Math Geosci, 42:1 (2009) 49-64. https://doi.org/10.1007/s11004-009-9257-x

[18] T. Mánik, B. Holmedal, Review of the Taylor ambiguity and the relationship between rate-independent and rate-dependent full-constraints Taylor models, Int J Plasticity, 55 (2014) 152-181. https://doi.org/10.1016/j.ijplas.2013.10.002